Asian Journal of Chemistry; Vol. 31, No. 12 (2019), 2875-2884

ASIAN JOURNAL OF CHEMISTRY

https://doi.org/10.14233/ajchem.2019.22272

Design, Synthesis, Computational and Biological Evaluation of 4-Amino-3,5-dimercapto-1,2,4-triazole Surface Functionalized Gold Nanoparticles

V. VEENA[1,*], K.H. SHIVAPRASAD[1], K.S. LOKESH[1], H. SHARANAGOUDA[2] and D. RAMAKRISHNA[3]

[1]Department of Chemistry, Vijayanagara Sri Krishnadevaraya University, Ballari-583105, India
[2]Department of Processing and Food Engineering, College of Agricultural Engineering, University of Agricultural Sciences, Raichur-584102, India
[3]Department of Biotechnology, Dayananda Sagar College of Engineering, Bangalore-560078, India

*Corresponding author: E-mail: veenaraj138@gmail.com; veena138n@gmail.com

Received: 16 June 2019; *Accepted*: 5 August 2019; *Published online*: 16 November 2019; AJC-19635

Gold nanoparticles (AuNPs) are an obvious choice for rapid advance in nanotechnology due to their amenability of synthesis, functionalization and less toxicity. Functionalization of AuNP surface with 4-amino-3,5-dimercapto-1,2,4-triazole (ADMT) ligand as ADMT-AuNPs was investigated with the aim to probe the suitability of innovative product to develop new antibacterial and anticancer strategies. Various characterization studies like UV-spectra, Zeta size, Zeta potential, XRD, SEM, TEM and FTIR results of AuNPs and ADMT-AuNPs have been performed to study the structural and electronic properties. The studies revealed that the functionalized nanoparticles are highly crystalline in nature with the sizes ranging between 20-22 and 50-55 nm for AuNPs and ADMT-AuNPs, respectively with FCC structures. The characterization data reveals that the synthesized nanoparticles are stable and presence of strong interactions between the metallic surface and the organic ligand. Further, ADMT-AuNPs showed good antibacterial activity against Gram-positive and Gram-negative bacteria. MTT assay exhibited the cell viability with an IC_{50} value of 45.32 % v/v for ADMT-AuNPs against breast adenocarcinoma (MCF-7) cell lines. Molecular characterization *i.e.*, *in silico* docking analysis helped in identifying and organizing the structural similarity/diversity at the molecular level. The *in silico* study indicated that the structure S1a has good glide score and glide energy for H-bonding among the possible conformations against bacterial and breast cancer protein. Molecular docking studies confirmed the introduction of conformational changes that are essential to surpass the potential energy barriers of ADMT-AuNPs for biocompatibility and proved that they hold a promising future in the medical field.

Keywords: Gold nanoparticles, 4-Amino-3,5-dimercapto-1,2,4-triazole, Antibacterial activity, Docking studies.

INTRODUCTION

Cancer malignancies and infections are the leading causes of death worldwide despite of the continuous improvements in the medications for curing and preventing cancer. This might be due to incessant evolution of antimicrobial resistance and drug-resistant cancer cells, which cannot be cured by conventional therapies [1]. Gold nanoparticles (AuNPs) with current innovative technologies present fascinating aspects to overcome the problems faced by conventional therapies [2-5]. The study of AuNPs provide an insight into their potential application related to size, electronic, magnetic, optical, assembly of multiple types and surface functionalization properties that are capable of producing quantum effects suitable for imaging, catalysis, sensing [6], non-linear optical devices [7], electron microscopy markers [8], DNA sequencing [9], plasmonics for chemotherapeutic drug delivery systems [10], photo-thermal therapy, immuno-chromatographic detection of pathogen in food and clinical specimen [11,12] and promote enormous growth of medicinal field with high speed which revolutionize the medicinal field. In fact, the size and the shape of AuNPs can be modified by tuning the synthetic protocols that makes them attractive for biomedical applications [13-16].

Reduction of gold solution using reducing agents [17-19], thermally [20], electrochemically [21], sonochemical decomposition [22], microwave assisted reduction [23] and green chemistry or biosynthesis [24-27] are available methods for the synthesis of AuNPs. Most commonly used is the wet chemical or chemical reduction method due to their versatility and ease for controlling size and shape [17-19]. Chemical reduction of

Au(III) derivatives such as aurochloric acid ($HAuCl_4$) in water to Au(0) using sodium citrate (Turkevich method) and sodium borohydride (Brust-Schiffrin method, which is two-phase synthesis) [28,29], hydroquinone reduction are more recently used techniques [30-34]. Common oxidation states of gold include +1 [Au(I) as aurous compounds) and +3 (Au(III) as auric compounds] but AuNPs however, exist in a non-oxidized state [Au(0)]. The ratio of gold salt to reducing agent, type of reducing agent, the stirring rate, the order of addition of the reagents, pH and temperature during the synthesis are the crucial factors that results in different sizes and shapes of the AuNPs [35,36].

Generally, AuNPs are easily produced in liquid chemical methods where in once all Au ions are reduced to Au atoms, the solution becomes supersaturated and leads to the formation of clusters of Au atoms or nucleus. Gradually Au nucleus absorbs further produced Au atoms, resulting in the growth until AuNPs coagulate and start to aggregate with time [37-40]. This affects the particles stability and dispersity very often limiting the shelf life of the AuNPs [28,41-43]. Therefore, the use of functionalizing/stabilizing agents alter wide range of characteristics on the surface, such as roughness [44], hydrophilicity [45], surface charge [46], surface energy, biocompatibility [47] and reactivity [48] by binding to the nanoparticles surface and prevents once formed AuNPs from further aggregation. Moreover, it has been demonstrated that AuNPs have strong binding affinity to certain ligands having thiols [49], disulfides [50], amines [51], nitriles, carboxylic acids, phosphine [52], porphyrins 1 [53], hyper branched polyethylenimine polymers [54] and biomolecules that has led to an extensive research effort investigating of biomedical applications.

Surface functionalization has been extensively studied and characterized in the last few decades with ligands like alkyl thiols and dialkyl disulphides which not only have greater affinity toward metal Au surfaces but also results in spontaneous monolayer's on Au substrates (self-assembled monolayers, SAMs) [51,55-58]. This is because gold-sulfur covalent bond or van der Waals interactions [59] are strong enough to facilitate the immobilization of thiol groups on the surface of metals. Thus, chemisorption energy of sulphydryl (RS-H) groups on Au or Au–S is found to be 126 kJ/mol and the energy of gold-sulfur bond has been reported as 418 kJ mol^{-1} [60]. In fact, addition of these alkyl thiols or dialkyl disulphides at the initial step during the synthesis, assist the sulphur (R-S) atoms to bind onto the surface of the nuclei and interact with the metal ions in solution. This affects the reaction equilibrium, the rate of particle nucleation and growth forming a stern layer on the particles which prevents aggregation and stops further growth [61-63]. Therefore hybrid nanomaterials obtained by thiol ligand functionalization of AuNPs have been used as platforms for building molecular recognition systems with both highly selective recognition properties for biomolecules and photonics.

The present study aimed at synthesis of novel AuNPs at the first stage through conventional Turkevich method modified by Fren's. Au-citrate shells are known to be weaker in nature due to electrostatic interaction of 4-amino-3,5-dimercapto-1,2,4-triazole ligand and surface. Thus, expecting to result in dimercapto-triazole functionalized AuNPs (ADMT-AuNPs). Further AuNPs and ADMT-AuNPs will be characterized by various techniques and subjected to biomedical applications like antibacterial and anticancer study on MCF-7 cell lines both quantitatively and qualitatively. Expected and possible bioactive conformations will be explored by molecular docking study, which is an effective channeling tool for further structural modification and designing of novel, possible structural model of ADMT-AuNPs.

EXPERIMENTAL

Gold chloride trihydrate (99.9 %, $HAuCl_4 \cdot 3H_2O$), tri-sodium citrate (99.5 %, $Na_3C_6H_5O_7 \cdot 2H_2O$), thiosemicarbazide, carbon disulphide, pyridine, hydrazine hydride and 3-(4,5-dimethylthiazole-2-yl)-2,5-diphenyltetrazolium bromide (MTT) were purchased from Sigma-Aldrich. For cell culture, culture medium and fetal calf serum (FCS) were purchased from Hi-Media, Mumbai, India and Invitrogen, USA. All other chemicals were purchased either from HiMedia, Mumbai, India or SRL, Mumbai, India. The bacterial strains were procured from the Microbial Type Culture Collection, Institute of Microbial Technology, Chandigarh, India. The MCF-7 cell lines were obtained from National Centre for Cell Science, Pune, India.

Synthesis of AuNPs: AuNPs were prepared by following the Fren's method [42]. An aqueous solution of $HAuCl_4$ (0.25 mM, 200 mL) was allowed to boil vigorously to its boiling point in an Erlenmeyer flask. Then 2 mL warm tri-sodium citrate (0.189 M) solution was quickly added with continuous stirring by means of magnetic flee, placed on a temperature controlled hot plate. The AuNPs formation was monitored as the colour changed from transparent light yellow to light red, scarlet or deep burgundy colour and finally to the characteristic wine red as all the Au ions were reduced. This mixture was boiled for an additional 20 min and then the resulting sol was cooled to room temperature with continuous stirring to enable complete reaction, yielding citrate-capped AuNPs. The concentration of the AuNPs was calculated using an established method and was found to be an approximately 3.0 nmol/L [64] assuming that all gold in the $HAuCl_4$ has been reduced.

Synthesis of 4-amino-3,5-dimercapto-1,2,4-triazole functionalized AuNPs (ADMT-AuNPs): 4-Amino-3,5-dimercapto-1,2,4-triazole (ADMT) was synthesized by using known method [65]. 200 mL of $HAuCl_4$ (0.25 mM) solution was added to 30 mL of 0.001 M ADMT solution slowly drop by drop placed on a temperature controlled hot plate with continuous stirring by means of magnetic flee. Then an aliquot of 2 mL tri-sodium citrate (0.189 M) solution was added to the boiling mixture. After the addition of citrate solution to the reaction mixture, the whole solution turns faint blue due to the interaction of functionalizing groups with Au ions and nucleation of nanoparticles. Then approximately after 70-75 s, blue colour suddenly changed into a brilliant deep red, indicating the formation of the ADMT functionalized AuNPs (ADMT-AuNPs). The heating was continued for 2 h to allow the complete exchange of the citrate molecules with ligand molecules. Later the suspension was allowed to stand for 24 h in dark before its use for further studies and checked for aggregation.

Antibacterial studies: The agar disc diffusion method was employed for the determination of antibacterial assay

of the synthesized AuNPs and ADMT-AuNPs [66]. The Petri plates containing media were solidified first and later incubated overnight to confirm that the Petri plates are free from contamination. These Petri plates were first inoculated with 0.1 mL from 10^8 cfu/mL of the seven pathogenic bacteria *Candida albicans, Escherichia coli, Staphylococcus aureus, Bacillus subtilis, Methicillin resistant Staphylococcus aureus, Listeria monocytogenes* and *Salmonella typhi* suspensions used as test organisms that were spread on different plates nourished with Muller Hinton agar media. Sterilized filter paper discs (5 mm in diameter) were loaded with synthesized AuNPs and ADMT-AuNPs (500 µg/disc) which were later impregnated on to disc containing test organisms. The comparative stability of discs containing gentamycin and nystatinin were analyzed simultaneously to evaluate their antibacterial susceptibility. Zones of inhibition were measured using Himedia scale after 24 h of incubation at 37 °C. All the experiments were performed in triplicate and results were recorded as mean ± standard deviation.

***in vitro* Study of dimercapto-triazole functionalized AuNPs (ADMT-AuNPs):** Cell viability was measured using MTT (3-(4,5-dimethyl thazole-2-yl)-2,5-diphenyl tetrazolium bromide) method [67]. The cell count was adjusted to 1.0×10^5 cells/mL using Dulbecco's modified eagle medium (DMEM) containing 10 % FBS. 200 µL of the diluted cell suspension (an approximately 15,000 cells/well) was added to each well of a 96 well micro titer plate. After 24 h, the supernatant was removed and the monolayer was washed with DMEM medium. Firstly 200 µL of increasing concentration of ADMT-AuNPs (0.1, 0.5, 1.0, 5.0, 10 & 20 % v/v) from stock sol was added and incubated for 24 and 48 h at 37 °C in 5 % CO_2 atmosphere. Later, 200 µL of 10 % MTT reagent was added to each well to get a final concentration of 0.5 mg/mL and the plates were gently shaken and incubated at 37 °C in 5 % CO_2 atmosphere for 24 and 48 h. The supernatant was removed and the resulting blue coloured formazan product formed was dissolved in 100 µL dimethyl sulfoxide (DMSO) solvent. The absorbance was measured using a micro plate reader at a wavelength 570 nm and also at 630 nm. Cisplatin was used as the standard anticancer drug for MCF-7 cell lines with an IC_{50} value of 25 µg/mL. Each experiment was performed in triplicate with duplicate plates. The percentage growth inhibition was calculated, after subtracting the background and the blank. Concentration of test drug needed to inhibit cell growth by 50 % (IC_{50}) was generated from the dose-response curve for the cell line.

***in silico* Analysis:** *in silico* is an expression that needs to be performed on computer or *via* computer simulation. ChemDraw software was used to draw the possible structures of ADMT-AuNPs. The 2D structures were then converted to a 3D structure data file, using the corina online 3D (3-Dimension) conversion server (https://www.mn-am.com/online_demos/corina_demo). Further, 3D structure of all compounds was optimized for docking conformation study. Thus generated three dimensional structure data files were used for molecular docking and interaction studies with bacteria β-lactamase toho-1 *Escherichia coli*-1iYS, *S. aureus* ligase (PDB ID: 1JIJ), cancer FHA2 domain of RAD53 (PDB ID: 1K2N), EGFR kinase domain (2j5f), Caspase-3 V266F (PDB ID: 5IAE) from the Protein Data Bank (RCSB) (http://www.rcsb.org/pdb) to study their antibacterial and anticancer activity. iGEMDOCKV2.1 software was used to study the protein-ligand nanoparticles interactions for all possible docking simulations [68]. The whole structure of the receptor was used for the molecular docking studies of ligand S1 and ADMT-AuNPs S1 (a-d). Further, the detailed interaction between best functional group and its position with the target proteins were analyzed in 3D visualization software PyMol [69].

RESULTS AND DISCUSSION

UV-visible analysis: The intensity and peak position of the LSPR (localized surface plasmon excitation) bands are known to be related to the diameter, size, morphology, dielectric properties and aspect ratio of metal nanoparticles [70]. Fig. 1a exhibits the colour of ADMT ligand solution, AuNPs

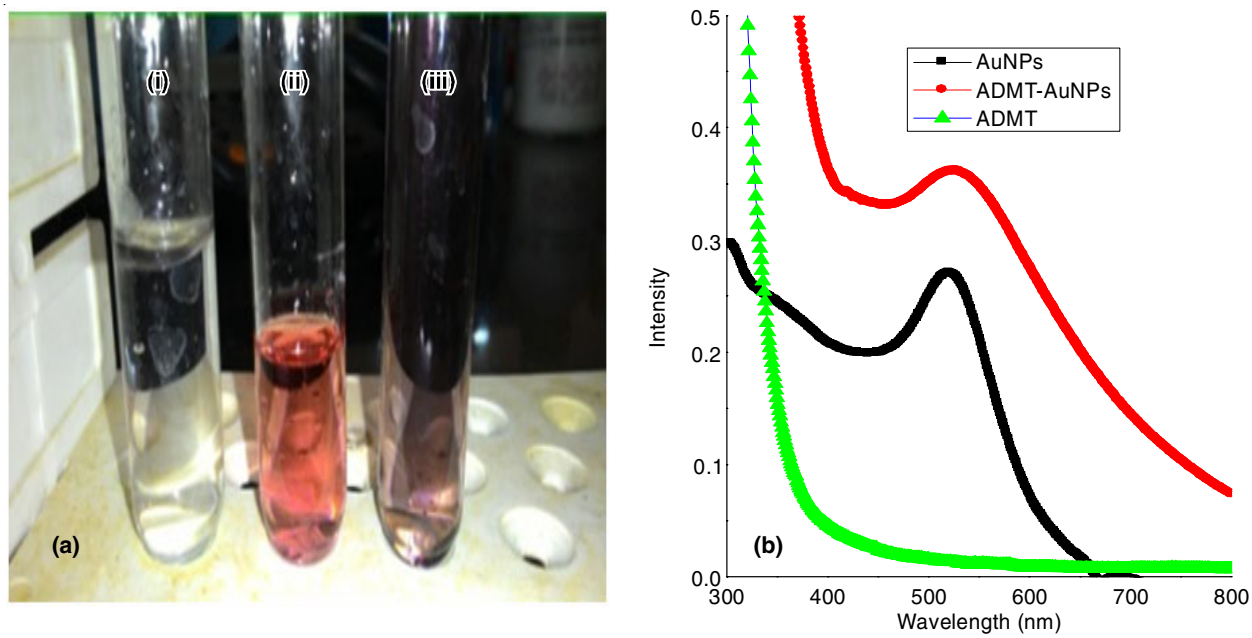

Fig. 1. (a) Colour for (i) ADMT, (ii) AuNPs and (iii) ADMT- AuNPs; (b) UV-visible spectra of ADMT, AuNPs and ADMT-AuNPs

(wine red sol) and ADMT-AuNPs (deeper wine red sol). Fig. 1b infers that ADMT ligand has no absorption peak in the visible region as it is a transluscent solution, whereas a strong absorption peak at 520 nm was observed for AuNPs and 540 nm for ADMT-AuNPs. Thus the red-shift (shift to longer wavelength region) of ADMT-AuNPs might be attributed to conjugation of ADMT ligand with AuNPs surface on functionalization. Red-shift of absorbance peak and peak broadening also indicate the larger average particle size of ADMT-AuNPs [71]. This confirms the functionalization of AuNPs to ADMT-AuNPs.

Particle size analysis: The resonance wavelength and bandwidth of nanoparticles are dependent on various factors like particle size, saturation solubility, dissolution velocity, physical stability and shape of nanoparticles, refractive indexof the surrounding medium, zeta potential, phase purity and mobility of the synthesized nanoparticles [72]. Zeta potential is the key parameter that indicates the degree of electrostatic repulsive forces present between similarly charged and adjacent nanoparticles present in the sol. This assists in governing the stability of synthesized AuNPs in a colloidal dispersion and the results are shown in Fig. 2 (Table-1).

DLS measurements supported the results obtained from UV-visible spectroscopy, yielding an average hydrodynamic diameter of 20-22 nm for AuNPs and 50-55 nm for ADMT-AuNPs. The big difference in size, zeta potential values, phase purity and mobility of AuNPs and ADMT-AuNPs (Fig. 2a and 2b) suggests that AuNPs are capped by certain functional groups present in the ADMT ligand. Tabulated values (Table-1) confirmed the formation of negative charges on the surface of AuNPs firstly by citrate that temporarily stabilizes AuNPs [37] but later collapses slowly with time. The low negative values of ADMT-AuNPs explains that it is highly stable compared to AuNPs. ADMT ligand brings greater electrostatic repulsion among AuNP surfaces leading to good phase purity and mobility of the medium in turn, leading to long term stability thus preventing aggregation.

XRD analysis: X-ray diffraction analysis (Fig. 3) gives the information about morphology, phase formation and purity of AuNPs and ADMT-AuNPs recorded in the range of 20 to 80° 2θ values.

The XRD pattern exhibited peaks at 2θ values of 37.04, 43.48, 64.54 and 72.95° that corresponds to the lattice planes (111), (200), (220) and (311) respectively. The intensity and the shape of the peaks are in good agreement with reference to unit cell of face centered cubic (FCC) phase of metallic Au nano crystals. All the peaks in the current XRD pattern matched with JCPDS data (JCPDS-PDF NO. 01-1172). The average size of AuNPs and ADMT-AuNPs were estimated using Debye-Scherer equation $D = 0.9\lambda/\beta \cos\theta$, where D is the diameter of the nanoparticles, β is the full width of half maxima (FWHM) of the peak in radians, θ is the diffraction angle and λ is wavelength of X-ray (1.540598 Å). The average size of the AuNPs was found to be about 20-22 nm (Fig. 3a) and 50-55 nm (Fig. 3b) for ADMT-AuNPs. Thus, the XRD pattern clearly demonstrates that they are highly crystalline in nature with less noise ratio proves their purity which are in good agreement with particle size analysis.

Scanning electron microscopy (SEM): A high resolution, scanning electron microscope operating at low electron voltage was used to photo image and characterize the surface of the AuNPs and ADMT-AuNPs as shown in Fig. 4. On closer inspection of the SEM images, it was observed that AuNPs (Fig. 4a) are polydispersed and slightly agglomerated. But the

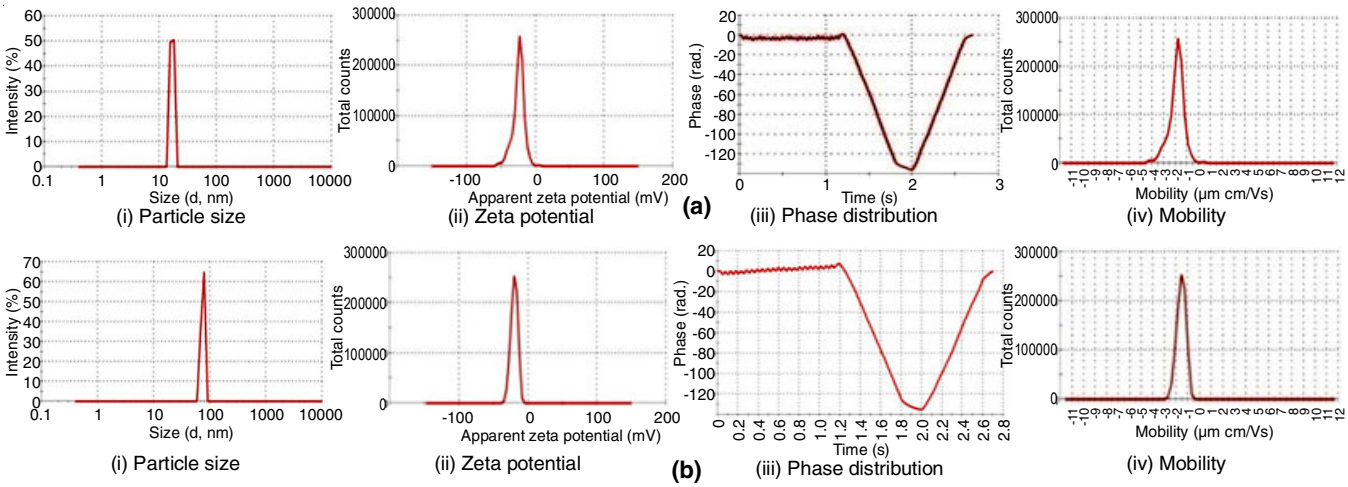

Fig. 2. Zeta particle size, phase distribution and mobility images of (a) AuNPs and (b) ADMT-AuNPs

TABLE-1
MEAN PARTICLE SIZE DIAMETER AND ZETA POTENTIAL RESULTS OF AuNPs AND ADMT-AuNPs

Parameters	AuNPs	ADMT-AuNPs
Z-average (nm)	20-21	50-51
Zeta potential (mV)	-24.1	-20.0
Zeta quality	Phase and distribution data is good	Phase and distribution data meets the quality criteria
Electrophoretic mobility (μm cm/Vs)	-1.890	-1.565
Mobility deviation (μm cm/Vs)	0.6626	0.3915
Conductivity (mS/cm)	0.338	0.220

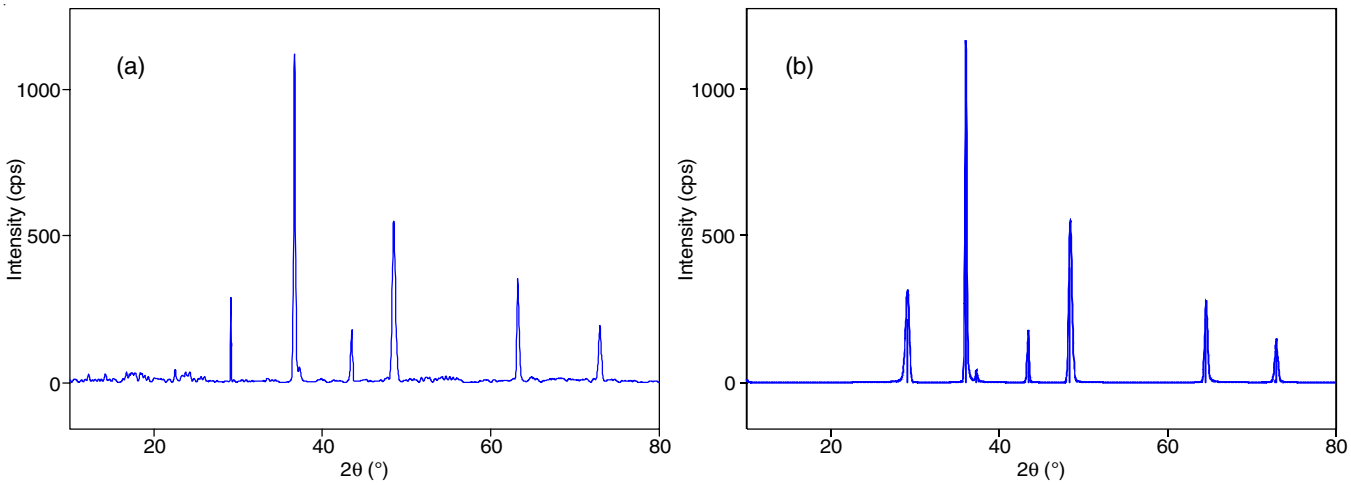

Fig. 3. XRD patterns of (a) AuNPs and (b) ADMT-AuNPs

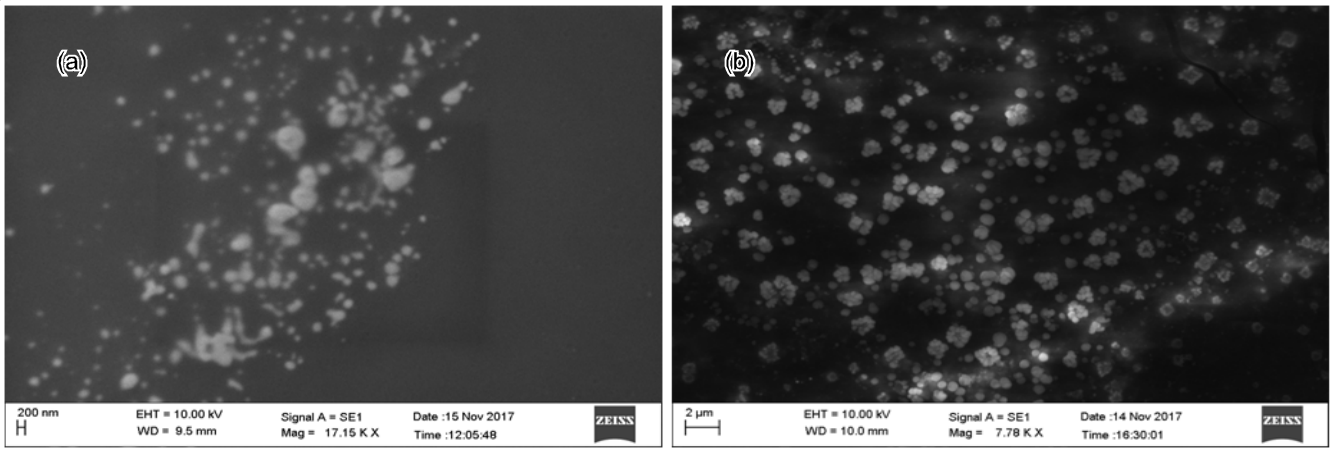

Fig. 4. SEM images of (a) AuNPs, (b) ADMT-AuNPs

particle size of ADMT-AuNPs are almost uniformly distributed and had cubic morphologies with merely round geometric circles. The space existing between ADMT-AuNPs might be due to steric repulsion of negative charges indicating the formation of ADMT-AuNPs.

TEM analysis: The morphology and internal crystalline structures of AuNPs and ADMT-AuNPs were studied by the high resolution transmission electron microscope and the selected area electron diffractions to find lattice planes of index (HRTEM and SAED) as shown in Fig. 5.

TEM microphotographs showed that AuNPs (Fig. 5a) are having particle size between 20-22 nm with some aggregation while ADMT-AuNPs (Fig. 5b) showed monodispersed particle size of 50-55 nm that seems to be cubic shaped without any aggregation. Narrow distribution of size might be due to the controlling of the uniform temperature distribution during the synthesis of ADMT-AuNPs [73,74]. The selected area electron diffraction (SAED) pattern (Fig. 5c and 5d) of AuNPs and ADMT-AuNPs showed four circular rings corresponding to (1 1 1), (2 0 0), (2 2 0) and (3 1 1) lattice planes confirming that they are highly crystalline in nature. The diffraction rings agreed with the JCPDS data (JCPPDS-PDF NO. 01-1172) with major indexing peaks (311). Thus (SAED) patterns confirmed the presence of elementals AuNPs which are in good agreement with the FCC crystallographic data results of XRD analysis.

FTIR analysis: In order to ensure the functionalization of AuNPs, FTIR spectra have been recorded. FTIR spectra of the triazole ligand was recorded and compared with AuNPs. FTIR results clearly revealed the presence of thiol group in the functionalized AuNPs. Thus the triazole plays an important role in the functionalization and stabilization of AuNPs by capping, which in turn prevents agglomeration.

The purified freeze dried powders of AuNPs were subjected to FTIR analysis to confirm the capping of ADMT to AuNPs (Fig. 6). In Fig. 6a, the broad band appearing at 3051.34 cm^{-1} can be assigned for the C-H stretching vibration, small stretching band at 3276.29 corresponds to NH_2 group, peak at 2360.28 cm^{-1} represents bending vibration of S-H (thiol) group, peak at 1596.63 cm^{-1} may be due to the presence of C=N bond, a sharp peak at 1287.20 cm^{-1} can be assigned to C-N bond, weak peak at 1010.54 cm^{-1} is due to the N-N bond and the broad peak at 1655.63 cm^{-1} may be due to the bending vibration of N-H group of ADMT ligand. The IR spectrum of ADMT-AuNPs (Fig. 6b) shows all the stretching and bending vibration peaks similar to ADMT ligand, except the absence of a peak at 2300 cm^{-1} range indicating S-H (thiol) group is involved in functionalization of AuNPs resulting ADMT-AuNPs. Thus the disappearance of S-H (thiol) group bending vibration and the decrease in intensity of the other bands are attributed to functionalization of AuNPs as ADMT-AuNPs.

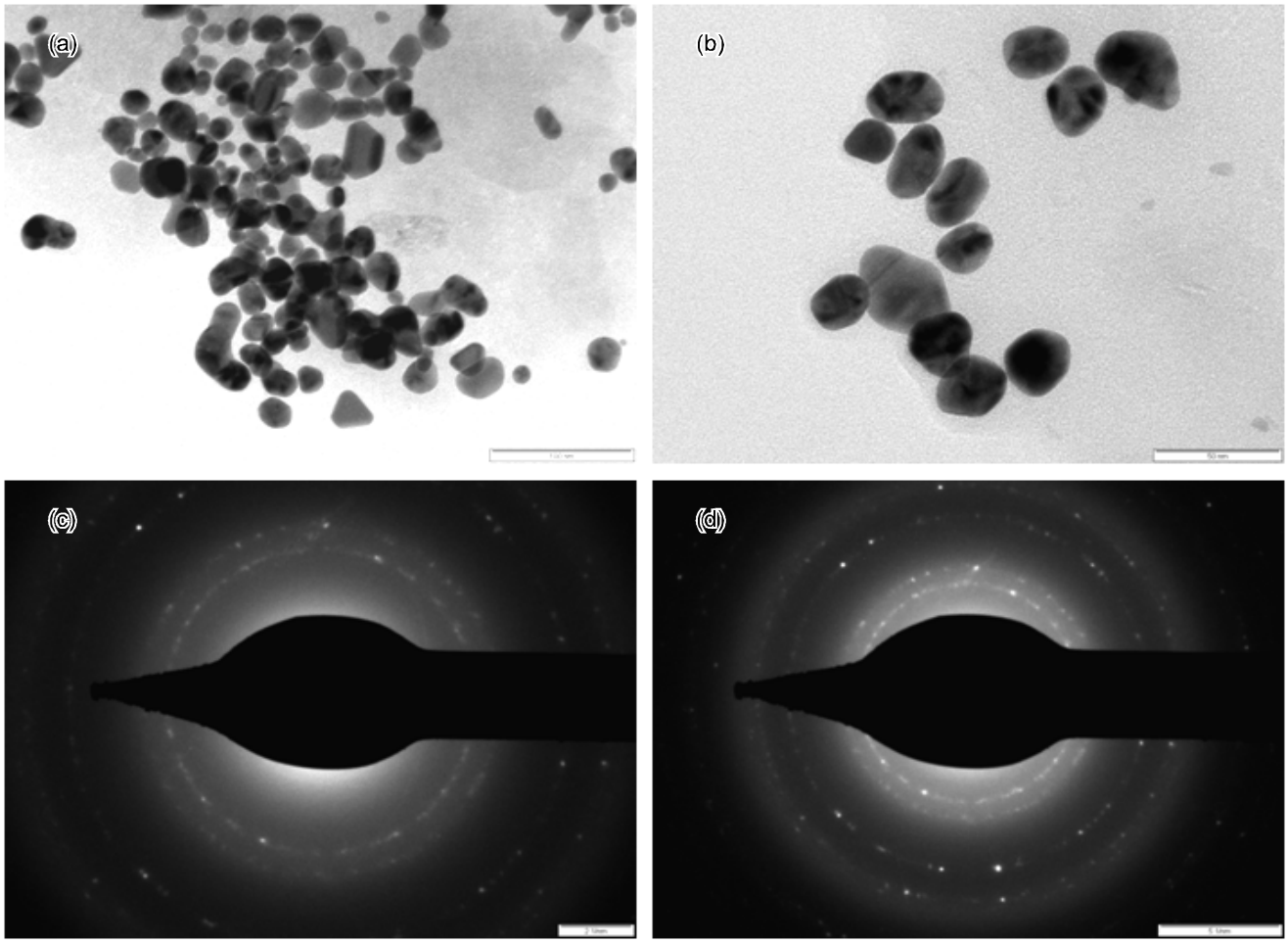

Fig. 5. TEM images of (a) AuNPs and (b) ADMT-AuNPs and SAD pattern of (c) AuNPs and (d) ADMT-AuNPs

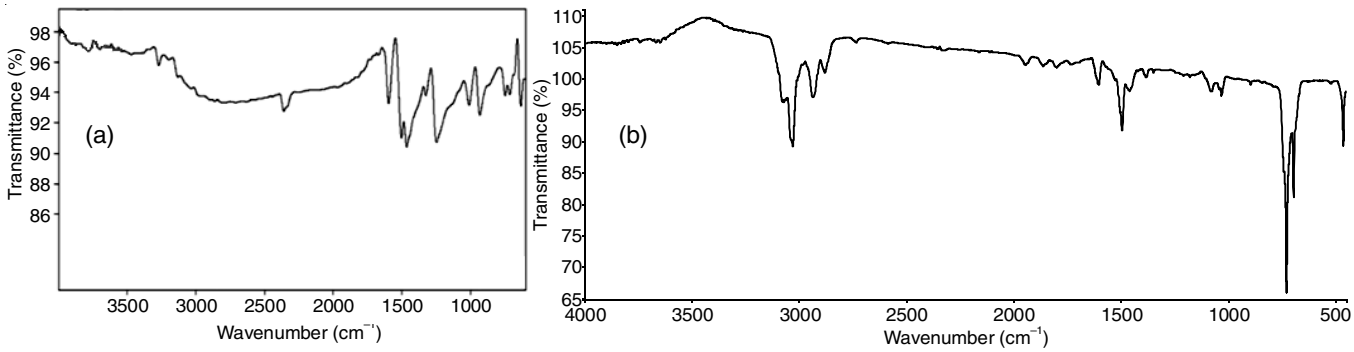

Fig. 6. FTIR spectra of (a) 4-amino-3,5-dimercapto-1,2,4-triazole (ADMT) (b) ADMT-AuNPs

Antibacterial assays with minimum inhibitory concentration: A significant deleterious effect on microbial growth was observed between AuNPs and ADMT-AuNPs. Evaluated antibacterial activity shows an important statistical difference in the zone of inhibition (mm) for both Gram-positive and Gram-negative micro-organisms (Table-2).

The antibacterial mechanism mainly depends on surface groups and the intrinsic properties of the nanoparticles that interact with bacterial species used for testing the assay. ADMT-AuNPs imprinted discs were observed to get aggregated as they come into contact with bacterial cells. Here the possible mechanism would be predicted as ADMT-AuNPs may have more ability to get penetrated into the bacterial cells and cause cell damage, followed by death [75]. Secondly, the functional groups of ADMT ligand that functionalizes AuNPs surface might be capable of attaching to the bacterial membrane by electrostatic interaction that causes cell wall distortions [76] and disrupt its integrity resulting in increased antibacterial activity compared to AuNPs.

***in vitro* Cytotoxicity test study of ADMT-AuNPs:** In this study, cytotoxicity of the synthesized ADMT-AuNPs were evaluated by MTT assay using MCF-7 cell lines. Reduction viability of the cell lines in a dose-dependent manner by ADMT-AuNPs is shown in Fig. 7(a-h).

The results demonstrated that the exposure of ADMT-AuNPs to MCF-7 cells alter morphology (an indication of

TABLE-2
ANTIBACTERIALACTIVITY OF AuNPs AND DIMERCAPTO-TRIAZOLE FUNCTIONALIZED (ADMT-AuNPs) (INHIBITION OF ZONE, mm)

Test human pathogens	AuNPs 500 µg/disc	ADMT-AuNPs 500µg/disc	Gentamicin 10 µg/disc	Nystatin 100 µg/disc
Candida albicans	17 ± 0.45	20 ± 0.15	ND	22 ± 0.65
Escherichia coli	18 ± 0.57	21 ± 0.27	28 ± 0.45	ND
Staphylococcus aureus	19 ± 0.64	22 ± 0.34	33 ± 0.69	ND
Bacillus subtilis	28 ± 0.12	29 ± 0.23	31 ± 0.23	ND
Methicillin resistant *Staphylococcus aureus*	11 ± 0.52	16 ± 0.57	32 ± 0.45	ND
Listeria monocytogenes	09 ± 0.78	10 ± 0.80	31 ± 0.63	ND
Salmonella typhi	10 ± 0.84	13 ± 0.86	30 ± 0.27	ND

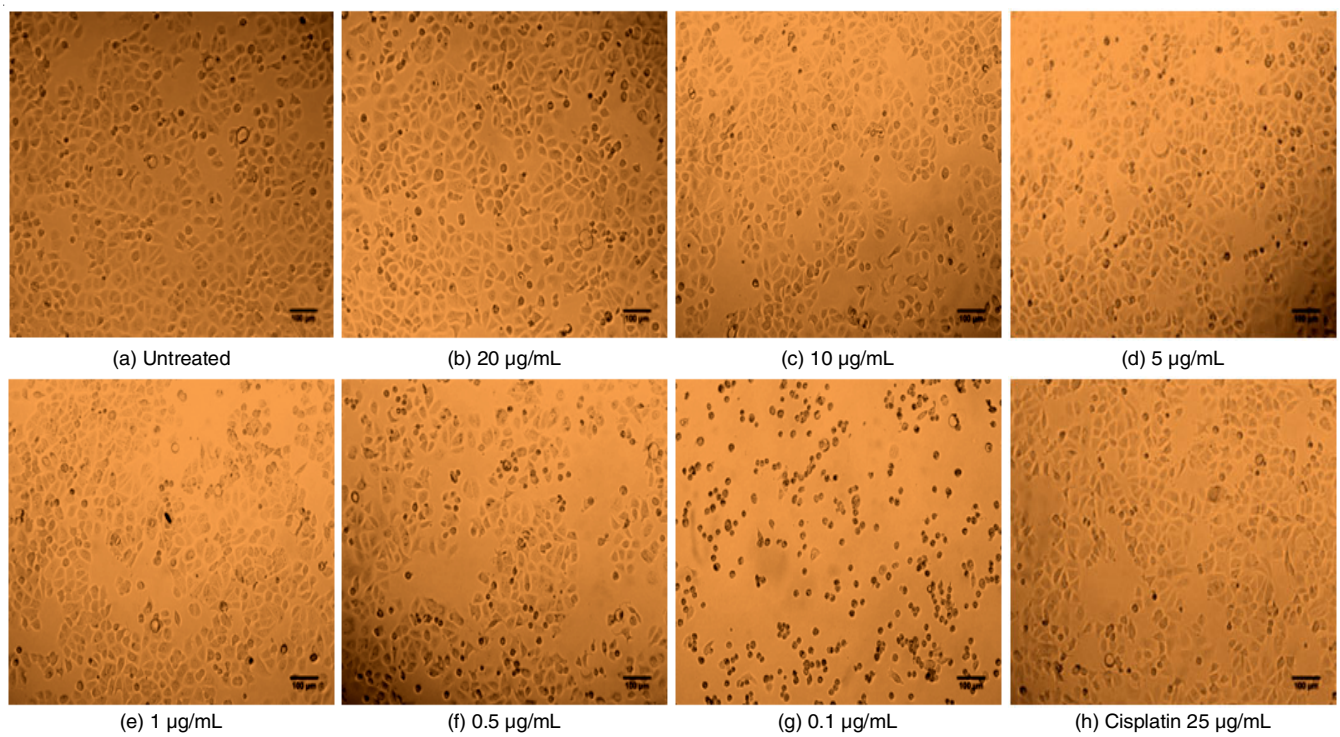

Fig. 7. Cytomorphological changes of MCF-7 cell line treated with colloidal AuNPs and ADMT-AuNPs

apoptosis) in the cancer cell lines which was assessed by staining and morphological changes (Fig. 7a-h). After incubation for 24 h with ADMT-AuNPs, the cells became round in appearance, exhibited nuclear condensation and significant nucleus fragmentation indicating apoptosis. It was also observed that apoptotic response of ADMT-AuNPs with MCF-7 cells increased at small dose which might be due to their higher solubility (capping of polar groups of ADMT ligand) and higher diffusion potential. The current study suggests that ADMT-AuNPs might induce apoptosis to MCF-7 cells by p53, bax/bcl-2 and caspase-3 as they are the common possible pathways for apoptosis [77,78]. Thus ADMT capping of AuNPs ensures greater uptake and retention by cancer cells.

Molecular docking: The molecular docking studies were employed to gain an insight into the mechanisms, interactions and to determine the contribution of site specific binding modes of ADMT-AuNPs. Absorption, distribution, metabolism, excretion and toxicity are the most important part of pharmacological studies. As ligands that posess good pharmacological and drug-likeness properties are very crucial for structure based drug discovery. Also the lead functional groups of molecules (drugs) and their interactions with cell proteins can be predicted by computational biology tools like molecular docking. The possible coordinates of ligand orientations and positions having 2D structure were converted to energy minimized 3D structures that favoured to bind with AuNPs are shown in Fig. 8. Finally, iGEMDOCK top ranking conformational structures of ADMT-AuNPs were visualized and one hundred independent docking runs were performed for each ADMT-AuNPs. The results of most favourable free energy of H-bonding are given in Table-3.

Computational docking studies were used after experimental measurements to further analyze the conformational changes induced by ADMT moiety. Ligand ADMT normally attaches to complementary charges on AuNPs and charged residues on the surface of proteins. As binding energy plays a vital role in docking studies, lowest binding energy compounds are considered as potent components in drug discovery to treat diseases. Thus, among the four possible conformations, S1a has least binding energy *i.e.*, -62.0388, -66.9393,-64.899 and -65.8501 for 1iYS, 1JIJ, 2j5f and 1K2N PDB respectively. The possible mechanism would be predicted as the ADMT ligand moiety gets distributed on the AuNPs surface resulting in increase of colloidal stability of zero valent ADMT-AuNPs with enhanced steric repulsion from adsorbed surfactants and

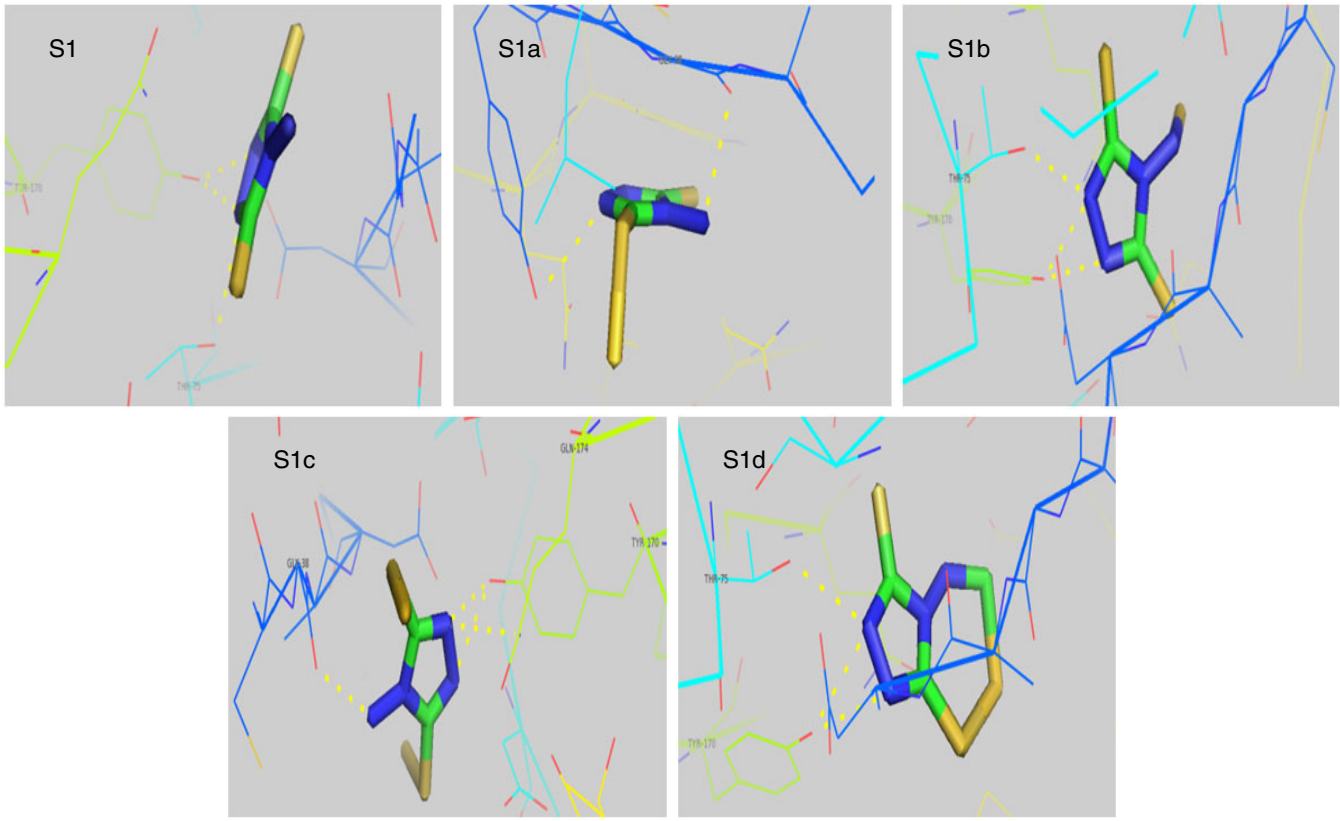

Fig. 8. Best and stable conformations of the synthesized ADMT as standard drug molecule and ADMT-AuNPs

TABLE-3
DOCKING RESULTS OF AuNPs AND ADMT-AuNPs

Compound name	1iYS (kcal/mol)	1JIJ (kcal/mol)	2j5f (kcal/mol)	1K2N (kcal/mol)
S1	-60.8836	-63.1473	-60.2055	-62.1064
S1a	-62.0388	-66.9393	-64.899	-65.8501
S1b	-61.2417	-64.9534	-64.448	-62.8608
S1c	-61.5473	-63.1862	-61.3212	-61.5162
S1d	-61.6125	-65.6577	-63.0613	-62.1765
Cisplatin	–	–	-27.6801	-27.716
Gentamycin	-98.2932	-91.5345	–	–

balanced by electrostatic forces. Surfactant molecules of ADMT with functional groups oriented to the AuNPs surface form a compact micellar layer. This layer might cause changes of membrane potential and decrease ATP levels within the cell and inhibit the binding of t-RNA with ribosomal subunit, affecting translation [79]. Another possibility is that ADMT-AuNPs can generate holes in the cell walls leading to leakage of cell contents and later bind with the DNA inhibiting transcription [80]. Thus, it is infered from the molecular modeling and docking studies that ADMT-AuNPs effectively bind to various protein binding sites that are crucial for mediating controlled growth inhibition of bacterial pathogenesis and cancer cell proliferation.

Conclusion

The ADMT-AuNPs have been successfully synthesized by modified Fern's method and were evaluated for antibacterial and anti-cancer potential against MCF-7 cell lines. The binding of ADMT to the surface of AuNPs at ambient temperature results in considerable surface modifications of AuNPs that result in ADMT-AuNPs. Interaction of ADMT on AuNP induces tertiary structural changes as both thiol and amine functional groups present in ADMT have affinity to AuNPs. The overall synthesis and characterization of ADMT-AuNPs exhibited sizes ranged between 20-22 nm (AuNPs) and 50-55 nm (ADMT-AuNPs) with FCC structures. Moreover, ADMT-AuNPs not only displayed excellent antibacterial property but also showed highly capable and significant anticancer activity against MCF-7 cell lines inducing cell cycle arrest and promote apoptosis. As ADMT-AuNPs exhibited a notable effect on cell proliferation at low quantity, could be a potential candidate for further *in vivo* study on cancer models. Docking models of ADMT-AuNP possible structures and H-bonding results indicated that they can easily reach the interior of proteins and chromophore residue surfaces that are prone to be affected by their interactions. Experimental and computational study results taken together concluded that ADMT-AuNPs have certain advantages like ease for applicability in large scale production, economically feasible, eco-friendly and biocompatible. Thus ADMT-AuNPs show major effects on structural tertiary for

future drug delivery applications as well as hold a promising future in the field of medicine and next generation of antimicrobials and anticancer agents.

ACKNOWLEDGEMENTS

The authors are thankful to Head, Department of Nanotechnology, UAS, Raichur, for providing the lab facilities for completion of synthesis and characterization work. The authors also acknowledge to DST-FIST(SR/FST/CSI-274/2016) for providing the financial support.

CONFLICT OF INTEREST

The authors declare that there is no conflict of interests regarding the publication of this article.

REFERENCES

1. J.N. Pendleton, S.P. Gorman and B.F. Gilmore, *Expert Rev. Anti Infect. Ther.*, **11**, 297 (2013); https://doi.org/10.1586/eri.13.12.
2. J.B. Delehanty, K. Boeneman, C.E. Bradburne, K. Robertson, J.E. Bongard and I.L. Medintz, *Ther. Deliv.*, **1**, 411 (2010); https://doi.org/10.4155/tde.10.27.
3. D.A. Giljohann, D.S. Seferos, W.L. Daniel, M.D. Massich, P.C. Patel and C.A. Mirkin, *Angew. Chem. Int. Ed.*, **49**, 3280 (2010); https://doi.org/10.1002/anie.200904359.
4. R.A. Petros and J.M. DeSimone, *Nat. Rev. Drug Discov.*, **9**, 615 (2010); https://doi.org/10.1038/nrd2591.
5. J. Shi, A.R. Votruba, O.C. Farokhzad and R. Langer, *Nano Lett.*, **10**, 3223 (2010); https://doi.org/10.1021/nl102184c.
6. M.-C. Daniel and D. Astruc, *Chem. Rev.*, **104**, 293 (2004); https://doi.org/10.1021/cr030698+.
7. P. Galletto, P.F. Brevet, H.H. Girault, R. Antoine and M. Broyer, *J. Phys. Chem. B*, **103**, 8706 (1999); https://doi.org/10.1021/jp991937t.
8. J. Fokkema, J. Fermie, N. Liv, D.J. van den Heuvel, T.O.M. Konings, G.A. Blab, A. Meijerink, J. Klumperman and H.C. Gerritsen, *Scient. Rep.*, **8**, Article No. 13625 (2018); https://doi.org/10.1038/s41598-018-31836-1.
9. W. Baschong and N.G. Wrigley, *J. Electron Microsc. Technol.*, **14**, 313 (1990); https://doi.org/10.1002/jemt.1060140405.
10. C.A. Mirkin, R.L. Letsinger, R.C. Mucic and J.J. Storhoff, *Nature*, **382**, 607 (1996); https://doi.org/10.1038/382607a0.
11. J.G. Holt, R.N. Krieg, P.H.A. Sneath and J.T. Staley, S.T. Williams Bergey's Manual of Determinative Bacteriology, Williams and Wilkins Baltimore, edn 9 (1994).
12. X. Huang, P.K. Jain, I.H. El-Sayed and M.A. El-Sayed, *Photochem. Photobiol.*, **82**, 412 (2006); https://doi.org/10.1562/2005-12-14-RA-754.
13. C.M. Niemeyer, *Angew. Chem.*, **113**, 4254 (2001); https://doi.org/10.1002/1521-3757(20011119)113:22<4254::AID-ANGE4254>3.0.CO;2-D.
14. A. Csaki, G. Maubach, D. Born, J. Reichert and W. Fritzsche, *Single Mol.*, **3**, 275 (2002); https://doi.org/10.1002/1438-5171(200211)3:5/6<275::AID-SIMO275>3.0.CO;2-0.
15. E. Katz, A.N. Shipway and I. Willner, ed.: G. Schmid, Biomaterial-Nanoparticle Hybrid Systems: Synthesis, Properties and Applications, in Nanoparticles-From Theory to Applications, Wiley-VCH: Weinheim, pp. 368-421 (2003).
16. W.J. Parak, D. Gerion, T. Pellegrino, D. Zanchet, C. Micheel, S.C. Williams, R. Boudreau, M.A.L. Gros, C.A. Larabell and A.P. Alivisatos, *Nanotechnology*, **14**, R15 (2003); https://doi.org/10.1088/0957-4484/14/7/201.
17. T. Pal, T.K. Sau and N.R. Jana, *Langmuir*, **13**, 1481 (1997); https://doi.org/10.1021/la960834o.
18. D.V. Goia and E. Matijevic, *New J. Chem.*, **22**, 1203 (1998); https://doi.org/10.1039/a709236i.
19. C.H. Munro, W.E. Smith, M. Garner, J. Clarkson and P.C. White, *Langmuir*, **11**, 3712 (1995); https://doi.org/10.1021/la00010a021.
20. K. Esumi, T. Tano, K. Torigoe and K. Meguro, *Chem. Mater.*, **2**, 564 (1990); https://doi.org/10.1021/cm00011a019.
21. M.L. Rodriguez-Sanchez, M.C. Blanco and M.A. Lopez-Quintela, *J. Phys. Chem. B*, **104**, 9683 (2000); https://doi.org/10.1021/jp001761r.
22. J. Zhu, S. Liu, O. Palchik, Y. Koltypin and A. Gedanken, *Langmuir*, **16**, 6396 (2000); https://doi.org/10.1021/la991507u.
23. I. Pastoriza-Santos and L.M. Liz-Marzan, *Langmuir*, **18**, 2888 (2002); https://doi.org/10.1021/la015578g.
24. S.P. Chandran, M. Chaudhary, R. Pasricha, A. Ahmad and M. Sastry, *Biotechnol. Prog.*, **22**, 577 (2006); https://doi.org/10.1021/bp0501423.
25. S.S. Shankar, A. Rai, A. Ahmad and M. Sastry, *Chem. Mater.*, **17**, 566 (2005); https://doi.org/10.1021/cm048292g.
26. A. Rai, A. Singh, A. Ahmad and M. Sastry, *Langmuir*, **22**, 736 (2006); https://doi.org/10.1021/la052055q.
27. B. Ankamwar, C. Damle, A. Ahmad and M. Sastry, *J. Nanosci. Nanotechnol.*, **5**, 1665 (2005); https://doi.org/10.1166/jnn.2005.184.
28. J. Turkevich, P.C. Stevenson and J. Hillier, *Discuss. Faraday Soc.*, **11**, 55 (1951); https://doi.org/10.1039/df9511100055.
29. M. Brust, M. Walker, D. Bethell, D.J. Schiffrin and R.J. Whyman, *J. Chem. Soc. Chem. Commun.*, **0**, 801 (1994); https://doi.org/10.1039/C39940000801.
30. M.S. Muthu and S. Singh, *Nanomedicine*, **4**, 105 (2009); https://doi.org/10.2217/17435889.4.1.105.
31. E. Duguet, S. Vasseur, S. Mornet and J.-M. Devoisselle, *Nanomedicine*, **1**, 157 (2006); https://doi.org/10.2217/17435889.1.2.157.
32. J.B. Hall, M.A. Dobrovolskaia, A.K. Patri and S.E. McNeil, *Nanomedicine*, **2**, 789 (2007); https://doi.org/10.2217/17435889.2.6.789.
33. D. Zhang, O. Neumann, H. Wang, V.M. Yuwono, A. Barhoumi, M. Perham, J.D. Hartgerink, P. Wittung-Stafshede and N.J. Halas, *Nano Lett.*, **9**, 666 (2009); https://doi.org/10.1021/nl803054h.
34. C.N.R. Rao, A. Müller and A.K. Cheetham, Nanomaterials–An Introduction, The Chemistry of Nanomaterials, Wiley-VCH Verlag GmbH & Co. KGaA, Weinheim, FRG, pp 1-11 (2005).
35. K.R. Brown, D.G. Walter and M.J. Natan, *Chem. Mater.*, **12**, 306 (2000); https://doi.org/10.1021/cm980065p.
36. M.N. Martin, J.I. Basham, P. Chando and S.-K. Eah, *Langmuir*, **26**, 7410 (2010); https://doi.org/10.1021/la100591h.
37. B.-K. Pong, H.I. Elim, J.-X. Chong, W. Ji, B.L. Trout and J.-Y. Lee, *J. Phys. Chem. C*, **111**, 6281 (2007); https://doi.org/10.1021/jp068666o.
38. J. Kimling, M. Maier, B. Okenve, V. Kotaidis, H. Ballot and A. Plech, *J. Phys. Chem. B*, **110**, 15700 (2006); https://doi.org/10.1021/jp061667w.
39. S.M. Saraiva and J.F. de Oliveira, *J. Dispers. Sci. Technol.*, **23**, 837 (2002); https://doi.org/10.1081/DIS-120015980.
40. J. Turkevich, *Gold Bull.*, **18**, 125 (1985); https://doi.org/10.1007/BF03214694.
41. P.J.G. Goulet and R.B. Lennox, *J. Am. Chem. Soc.*, **132**, 9582 (2010); https://doi.org/10.1021/ja104011b.
42. G. Frens, *Nature Phys. Sci.*, **241**, 20 (1973); https://doi.org/10.1038/physci241020a0.
43. M.K. Chow and C.F. Zukoski, *J. Colloid Interface Sci.*, **165**, 97 (1994); https://doi.org/10.1006/jcis.1994.1210.
44. R.V. Lapshin, A.P. Alekhin, A.G. Kirilenko, S.L. Odintsov and V.A. Krotkov, *J. Surf. Invest. X-ray, Synchrotron Neutron Tech.*, **4**, 1 (2010); https://doi.org/10.1134/S1027451010010015.

45. A.P. Alekhin, G.M. Boleiko, S.A. Gudkova, A.M. Markeev, A.A. Sigarev, V.F. Toknova, A.G. Kirilenko, R.V. Lapshin, E.N. Kozlov and D.V. Tetyukhin, *Nanotechnol. Russ.*, **5**, 696 (2010); https://doi.org/10.1134/S1995078010090144.
46. S. Bertazzo and K. Rezwan, *Langmuir*, **26**, 3364 (2009); https://doi.org/10.1021/la903140k.
47. S. Bertazzo, W.F. Zambuzzi, H.A. da Silva, C.V. Ferreira and C.A. Bertran, *Clin. Oral Implants Res.*, **20**, 288 (2009); https://doi.org/10.1111/j.1600-0501.2008.01642.x.
48. G. London, K.-Y. Chen, G.T. Carroll and B.L. Feringa, *Chem. Eur. J.*, **19**, 10690 (2013); https://doi.org/10.1002/chem.201300500.
49. R.C. Doty, T.R. Tshikhudo, M. Brust and D.G. Fernig, *Chem. Mater.*, **17**, 4630 (2005); https://doi.org/10.1021/cm0508017.
50. A. Ulman, *Chem. Rev.*, **96**, 1533 (1996); https://doi.org/10.1021/cr9502357.
51. M. Schulz-Dobrick, K.V. Sarathy and M. Jansen, *J. Am. Chem. Soc.*, **127**, 12816 (2005); https://doi.org/10.1021/ja054734t.
52. E. Ramirez, S. Jansat, K. Philippot, P. Lecante, M. Gomez, A.M. Masdeu-Bulto and B. Chaudret, *J. Organomet. Chem.*, **689**, 4601 (2004); https://doi.org/10.1016/j.jorganchem.2004.09.006.
53. A. Kotiaho, R. Lahtinen, A. Efimov, H. Lehtivuori, N.V. Tkachenko, T. Kanerva and H. Lemmetyinen, *J. Photochem. Photobiol. Chem.*, **212**, 129 (2010); https://doi.org/10.1016/j.jphotochem.2010.04.005.
54. H.W. Duan and S.M. Nie, *J. Am. Chem. Soc.*, **129**, 2412 (2007); https://doi.org/10.1021/ja067727t.
55. N. Camillone III, C.E.D. Chidsey, G.-Y. Liu, T.M. Putvinski and G. Scoles, *J. Chem. Phys.*, **94**, 8493 (1991); https://doi.org/10.1063/1.460082.
56. L.H. Dubois and R.G. Nuzzo, *Annu. Rev. Phys. Chem.*, **43**, 437 (1992); https://doi.org/10.1146/annurev.pc.43.100192.002253.
57. H.A. Biebuyck, C.D. Bain and G.M. Whitesides, *Langmuir*, **10**, 1825 (1994); https://doi.org/10.1021/la00018a034.
58. F. Schreiber, *Prog. Surf. Sci.*, **65**, 151 (2000); https://doi.org/10.1016/S0079-6816(00)00024-1.
59. J.J. Gooding, F. Mearns, W. Yang and J. Liu, *Electroanalysis*, **15**, 81 (2003); https://doi.org/10.1002/elan.200390017.
60. D.R. Lide, Handbook of Chemistry and Physics, CRC Press: Boca Raton, FL, USA, edn 82 (2001).
61. P.C. Ray, *Chem. Rev.*, **110**, 5332 (2010); https://doi.org/10.1021/cr900335q.
62. C.B. Murray, C.R. Kagan and M.G. Bawendi, *Science*, **270**, 1335 (1995); https://doi.org/10.1126/science.270.5240.1335.
63. C.B. Murray, S. Sun, W. Gaschler, H. Doyle, T.A. Betley and C.R. Kagan, *IBM J. Res. Develop.*, **45**, 47 (2001); https://doi.org/10.1147/rd.451.0047.
64. Z.L. Jiang, Z.W. Feng, Y.S. Li, F. Li, F.X. Zhong, J.Y. Xie and X.H. Yi, *Sci. China B Chem.*, **44**, 175 (2001); https://doi.org/10.1007/BF02879535.
65. P.C. Guha and S.C. De, *J. Chem. Soc.*, **125**, 1218 (1924); https://doi.org/10.1039/CT9242501215.
66. S. Pal, Y.K. Tak and J.M. Song, *Appl. Environ. Microbiol.*, **73**, 1712 (2007); https://doi.org/10.1128/AEM.02218-06.
67. M.C. Alley, MTT Cell Proliferation Assay Instruction Guide-ATCC, VA, USA.
68. T. Neema, P. Kumud and P. Bhasker, *Int. J. PharmTech. Res.*, **7**, 156 (2015).
69. M.A. Lill and M.L. Danielson, *J. Comput. Aided Mol. Discov.*, **25**, 13 (2011); https://doi.org/10.1007/s10822-010-9395-8.
70. D. Philip, *Spectrochim. Acta A, Mol. Biomol. Spectrosc.*, **71**, 80 (2008); https://doi.org/10.1016/j.saa.2007.11.012.
71. S. Shankar, A. Rai, A. Ahmad and M. Sastry, *J. Colloid Interface Sci.*, **275**, 496 (2004); https://doi.org/10.1016/j.jcis.2004.03.003.
72. R.S. Patil, R.M. Kokate, C. Jambhale, S. Pawar, S. Han and S. Kolekar, *Adv. Nat. Sci. Nanosci. Nanotechnol.*, **3**, 015013 (2012); https://doi.org/10.1088/2043-6262/3/1/015013.
73. D.N. Furlong, A. Launikonis, W.H.F. Sasse and J.V. Sanders, *J. Chem. Soc., Faraday Trans. I*, **80**, 571 (1984); https://doi.org/10.1039/f19848000571.
74. E.M.S. Azzam, A.M. Badawi, A.R.E. Alawady and A. Soliman, *J. Dispers. Sci. Technol.*, **30**, 540 (2009); https://doi.org/10.1080/01932690802553932.
75. M.R. Bindhu and M. Umadevi, *Mater. Lett.*, **120**, 122 (2014); https://doi.org/10.1016/j.matlet.2014.01.108.
76. M.F. Zawrah and S.I. Abd El-Moez, *Life Sci. J.*, **8**, 37 (2011).
77. M. Fritsche, C. Haessler and G. Brandner, *Oncogene*, **8**, 307 (1993).
78. R.J. Youle and A. Strasser, *Nat. Rev. Mol. Cell Biol.*, **9**, 47 (2008); https://doi.org/10.1038/nrm2308.
79. Y. Cui, Y. Zhao, Y. Tian, W. Zhang, X. L and X. Jiang, *Biomaterials*, **33**, 2327 (2012); https://doi.org/10.1016/j.biomaterials.2011.11.057.
80. A. Rai, A. Prabhune and C.C. Perry, *J. Mater. Chem.*, **20**, 6789 (2010); https://doi.org/10.1039/c0jm00817f.